

IR 78-1577

EA-6010-16

Dist. Category UC-90C

MATERIALS RESEARCH FOR CLEAN UTILIZATION OF COAL

QUARTERLY PROGRESS REPORT

April - June 1978

Samuel J. Schneider
Project Manager

Center for Materials Science
National Bureau of Standards
Washington, D. C. 20234

PREPARED FOR THE UNITED STATES
DEPARTMENT OF ENERGY

Under Contract No. EA-77-A-01-6010

"This report was prepared as an account of work sponsored by the United States Government. Neither the United States nor the United States Department of Energy, nor any of their employees, nor any of their contractors, subcontractors, or their employees, makes any warranty, express or implied, or assumes any legal liability or responsibility for the accuracy, completeness, or usefulness of any information, apparatus, product or process disclosed, or represents that its use would not infringe privately owned rights."

TABLE OF CONTENTS

	PAGE
I. OBJECTIVE AND SCOPE OF WORK.	1
II. SUMMARY OF PROGRESS TO DATE.	1
Articles Published and Talks Presented	4
III. DETAILED DESCRIPTION OF TECHNICAL PROGRESS	5
1. Metal Corrosion.	5
a. Slow Strain Rate Test.	5
b. Pre-Cracked Fracture Test.	14
2. Ceramic Deformation, Fracture and Erosion.	16
3. Chemical Degradation	27
a. Reactions and Transformations.	27
b. Slag Characterization.	35
c. Vaporization and Chemical Transport.	41
4. Failure Prevention	44
a. Failure Information Center	44
b. Materials Properties Data Center	47

I. OBJECTIVE AND SCOPE OF WORK

Coal Gasification processes require the handling and containment of corrosive gases and liquids at high temperature and pressures, and also the handling of flowing coal particles in this environment. These severe environments cause materials failures which inhibit successful and long-time operation of the gasification systems. The project entails investigations on the wear, corrosion, chemical degradation, fracture, and deformation processes which lead to the breakdown of metals and ceramics currently being utilized in pilot plants. Studies will also be carried out on new candidate materials considered for improved performance. Special emphasis will be devoted to the development of test methods, especially short-time procedures, to evaluate the durability of materials in the gasification environments. These methods will focus on wear, impact erosion, stress corrosion, strength, deformation, slow crack growth and chemical degradation. A system has been initiated to abstract and compile all significant operating incidents from coal conversion plants as well as materials property and performance information important to the design and operation of these plants. This program will provide a central information center where problems of common interest can be identified and analyzed to avoid unnecessary failures and lead to the selection of improved materials for coal conversion and utilization. Active consultation to DOE and associated contractors will be provided as requested.

II. SUMMARY OF PROGRESS TO DATE

Brief Summary

1. Metal Corrosion

a. Constant Strain-Rate Test

The wedge-loaded DCB specimens exposed in the Synthane plant in the liquid phase scrubber surge tank were further evaluated by splitting them apart and measuring the crack length. Type 310 SS, Type 309 SS, and nickel alloy 800 showed no crack growth during the test. Type 304 SS, Type 446 SS, and nickel alloy 671 showed only very minimal crack growth (175 μ m to 775 μ m). Low carbon steel (AISI 1015-20) exhibited a crack growth of 2.63 cm. Coating the Type 310 SS tensile specimens with nickel or copper increased the ductility (elongation and reduction in area) of Type 310 SS as compared to a smooth or glass-beaded Type 310 SS specimen when tested at 600 °C in helium at a strain rate of 10^{-6} /s. The results of testing Type 310 SS in air at 600 °C at a strain rate of 10^{-6} /s show that the ductility (elongation and reduction in area) are very similar to results obtained when tested in argon, helium, or simulated coal conversion gases. Several Type 309 SS specimens, which are similar in composition to Type 310 SS except for lower nickel and chromium contents and higher silicon content, were tested at 600 °C (in argon, helium, and simulated coal conversion gas) at strain rates of 10^{-6} /s and lower and were found to be much more ductile than Type 310 SS when tested under the same conditions. No cracking was observed in any of the Type 309 SS specimens tested.

Some limited testing of alloys will be done, but the preparation of the final summary report on the test method will take precedence during the next quarter.

b. Pre-Cracked Fracture Tests

Development and analysis of the tension loaded double cantilever beam stress corrosion specimen has continued. Experimental tests to verify the analysis and to test for the susceptibility to cracking were initiated.

2. Ceramic Deformation, Fracture and Erosion

Construction and assembly of the high-pressure, high-temperature mechanical loader was completed this quarter with the installation and checkout of the pressure balancing system. In addition, the elevated temperature properties of two low-alumina refractory concretes both before and after hydrothermal exposure were investigated. Mineral phase changes were monitored by x-ray diffraction techniques at room temperature after the hot flexural strength determination.

Final evaluation of the high-pressure, high-temperature mechanical loader will be undertaken. This evaluation mainly involves establishing the operating characteristics of the pressure-balancing system and the load application system in the presence of an applied pressure. Exposure studies will begin for a high and a low-alumina refractory concrete in a 60% H₂O - 40% H₂ environment.

3. Chemical Degradation

a. Reactions and Transformations

Energy dispersive powder diffraction patterns obtained in three series of experiments with an unfired bar of high-alumina neat cement heated in steam have been interpreted. Initially, the specimen consisted of CA and α -A with small amounts of CAH₁₀, C₂AH₈, C₃AH₆, and AH. Of the reactions observed, the hydration of α -A to form AH, and the subsequent dissociation of AH at higher temperatures are among the most important. These reactions, which are believed to have an important effect on the strength of high alumina castable refractories have been observed in real time by the *in situ* x-ray diffraction method, and the progress of the reactions has been plotted.

During the next quarter NBS refractory A-56 with mullite aggregate, as well as the bonding matrix of A-56, are to be tested in steam. Additional work on specimens of neat cement is also planned.

b. Slag Characterization

The vertical temperature profile of the molten slag was determined in steam. A uniform temperature profile was found in the central portion

of the crucible, and it was concluded that this is where the actual temperature must be measured.

It is planned to construct a new drag cup assembly allowing direct temperature measurement of the molten slag.

c. Vaporization and Chemical Transport

Evidence of non-equilibrium chemical reaction effects has been noted for systems involving H₂O as a gaseous reactant and either sodium calcium silicate or sodium sulfate molten substrate. The new capillary probe sampling device has been calibrated and shown to faithfully sample equilibrium vaporization systems.

Results obtained to date will be checked, and extended where necessary, for presentation and publication at the 10th Materials Research Symposium on Characterization of High Temperature Vapors.

4. Failure Prevention

a. Failure Information Center

Thirty-two additional reports of operating experiences and failure analysis reports were entered into the Center's data base. Over two hundred information items were transmitted to plant operators and fossil energy contractors. Additional progress was made in completing the detailed report covering the performance of materials and components used in the Conoco lignite gasification pilot plant. The Center's data base is being revised in format and content to aid in future information dissemination.

b. Materials Properties Data Center

The regular activities of the Data Center have gained momentum with the submission to DoE of the first Data Summaries of contractor's research projects, the delivery of ordered computer-terminal equipment, increasing activity with respect to learning about the equipment capabilities, the choice of a Data Base Management System and more intensive study of data base design with respect to the chosen system, and the arrangement to test the Management System with respect to the services of two vendors of the system.

Articles Published and Talks Presented

"X-ray Powder Diffraction Measurements in Reactive Atmospheres at 1000 °C and 7 Mpa," F. A. Mauer and C. R. Robbins. Accepted for publication in Advances in X-ray Analysis, Vol. 22.

"Hot Strength and Fracture Toughness of an Anorthite-Bonded Refractory," J. M. Bukowski, May 6-11, 1978, American Ceramic Society Meeting - Refractories Properties and Testing, Detroit, Michigan.

"Erosion of Castable Refractories," S. M. Wiederhorn, 14th Annual Symposium on Refractories, April 1978, St. Louis, Mo.

III. DETAILED DESCRIPTION OF TECHNICAL PROGRESS

1. Metal Corrosion

a. Slow Strain Rate Test (G. M. Ugiansky and C. E. Johnson, 561.00)

Progress: The wedge-loaded DCB specimens exposed in the Synthane plant in the liquid phase scrubber surge tank (mentioned previously in the March 1978 Quarterly Report) were further evaluated by splitting them apart and measuring the crack length. These specimens had been exposed for a combined time of 2046 hours (592 hours operating time and 1454 hours standby time) at an average operating temperature of 196°C (385°F) and a pressure of 600 psig. Type 310 SS, Type 309 SS, 304 SS, Type 446 SS, and nickel alloy 671 showed only very minimal crack growth (175µm to 775µm). Low carbon steel (AISI 1015-20) exhibited a crack growth of 2.63 cm. Although the test temperature may not have been high enough to have had a detrimental effect on the stainless steel specimens, it was high enough to cause some stress relief of the specimens; thus, reducing the initial load on the specimen.

In the laboratory slow strain rate testing, several Type 310 SS specimens were run in air and in an inert atmosphere of helium at 600°C and a strain rate of 10^{-6} /s (Table 1). Several different surface preparations of the Type 310 SS specimens were investigated from the point of view of keeping the environment away from the specimen so that a base line (that is, properties without environmental interaction) could be determined. On one of the Type 310 SS specimens the reduced section was glass-beaded to alter the surface structure to see if this would affect the surface cracking previously seen in Type 310 SS under the same test conditions. The glass-beaded Type 310 SS specimen fractured in a brittle manner (Table I) with many secondary cracks - much like the previously tested smooth tensile specimens of 310 SS. Another Type 310 SS specimen was plated with a 62.5µm layer of nickel to see if this would act as a barrier layer to prevent any environmental interaction with the specimen. This specimen failed with slightly higher ductility (Table I) than the glass-beaded specimen but several cracks were apparent through the nickel layer (Fig. 1). Another Type 310 SS specimen was plated with 100µm of copper to see if this layer would act as a getter for oxygen thus preventing any environmental interaction with the specimen. This specimen was less susceptible to cracking (had higher ductility) than both the glass-beaded and nickel plated specimens (Table I). Only a few cracks were visible through the copper layer (Fig. 1). The differences in ductility of the glass beaded, nickel plated, and copper plated 310 SS specimens are apparent from the stress-strain curves in Fig. 2. Even though there is still some cracking in the Type 310 SS specimens, the plating of nickel and copper has greatly increased the ductility of these specimens. It is not

known at this time as to whether the plated coatings have acted as complete barriers to prevent any interaction of the environment and the Type 310 SS material since there is still a possibility of diffusion through the coatings. With the coatings the ductility of Type 310 SS has increased when tested in helium, which may contain a low partial pressure of O_2 and/or H_2O , at $600^\circ C$ at a strain rate of $10^{-6}/s$. (The manufacture specifications indicates 0.1-0.5% O_2 and 2-250 ppm H_2O contents.)

Another Type 310 SS specimen was tested in air at $600^\circ C$ at a strain rate of $10^{-6}/s$. The results are shown in Table 1. The elongation and reduction in area results for the Type 310 SS tested in air at $600^\circ C$ are similar to the results obtained for the same alloy tested in helium, in the oxidizing/sulfidizing simulated coal conversion gas, and in the oxidizing/sulfidizing/carburizing simulated coal conversion gas. It appears that if oxygen does play a part in the cracking of Type 310 SS when tested at $600^\circ C$ at a strain rate of $10^{-6}/s$ then only a minimum amount is necessary and any larger amount does not have any further detrimental effect.

Several Type 309 SS specimens were tested at $600^\circ C$ in different environments and strain rates (Table I). Type 309 SS is similar in composition to Type 310 SS except for lower nickel and chromium contents and higher silicon content (Table 2). The results of testing Type 309 SS in argon at a strain rate of $10^{-6}/s$ are shown in Table 1 and Fig. 3. The Type 309 SS specimen remained ductile with no cracking; whereas, Type 310 SS cracked* and was less ductile when tested under the same conditions. A Type 309 SS specimen tested in helium at $600^\circ C$ at a strain rate of $10^{-6}/s$ had even higher ductility (elongation and reduction in area) than the 309 SS specimen tested in argon (Table 1). A comparison of stress-strain curves of Type 309 SS and Type 310 SS tested in helium at $600^\circ C$ and at a strain rate of $10^{-6}/s$ is shown in Fig. 4. Type 309 SS remained ductile even when tested at a slower strain rate of $5 \times 10^{-7}/s$ at $600^\circ C$ in helium (Table 1). No cracking was apparent in the Type 309 SS specimen tested at this slower strain rate of $5 \times 10^{-7}/s$. Type 309 SS also remained ductile with no cracking when tested in the oxidizing/sulfidizing/carburizing simulated coal gasification environment (Table 1). The microstructure of the Type 309 SS was found to contain some ferrite which could contribute to the higher ductility than was seen in the Type 310 SS where no ferrite was found. The higher silicon content and greater chromium to nickel ratio in the Type 309 SS, as compared to Type 310 SS, could promote the formation of the ferrite. The existence of ferrite could account for sigma phase formation except that the test temperature of $600^\circ C$ does not seem to be great enough for sigma formation. In summary, the slow strain rate test indicates that the Type 309 SS performs better than the Type 310 SS. Since Type 309 SS has all of the necessary properties of Type 310 SS for coal conversion application but appears to be less susceptible

*See January-March 1978 Quarterly Report.

to stress cracking, these results may be of great significance. Their implications should be looked into further.

Plans: Some limited testing of alloys will be done, but the preparation of the final report will take precedence.

Slow Strain Rate Test Results

TABLE 1

<u>Specimen</u>	<u>Test Environment</u>	<u>Tensile Strength</u>		<u>Elongation</u>	<u>Reduction</u>
		<u>MPa</u>	<u>(psi)</u>	<u>%</u>	<u>in Area, %</u>
Glass-beaded 310 SS	Helium	343	(51,200)	12.5	19.2
Nickel plated 310 SS	Helium	327	(47,400)	22.6	31.2
Copper plated 310 SS	Helium	301	(43,600)	27.6	33.9
310 SS	Air	-	-	17.1	26.0
#1 309 SS	Tank Argon	323	(46,800)	31.2	57.1
#2 309 SS	Helium	334	(48,400)	37.7	69.2
#3 309 SS*	Helium	-	-	34.3	62.1
#4 309 SS	O-S-C ⁺	-	-	36.5	62.7

*Tested at a strain rate of 5×10^{-7} /s.

⁺O-S-C: oxidizing-sulfidizing-carburizing simulated coal gasification environment.

Alloy Composition, Wt%

TABLE 2

	<u>309 SS</u>	<u>310 SS</u>
Carbon	0.07%	0.08%
Manganese	1.74	1.76
Phosphorus	0.018	0.027
Sulfur	0.013	0.021
Silicon	0.70	0.48
Nickel	13.22	19.66
Chromium	22.96	24.83
Molybdenum	0.08	0.10
Copper	0.07	0.17
Iron	Bal	Bal

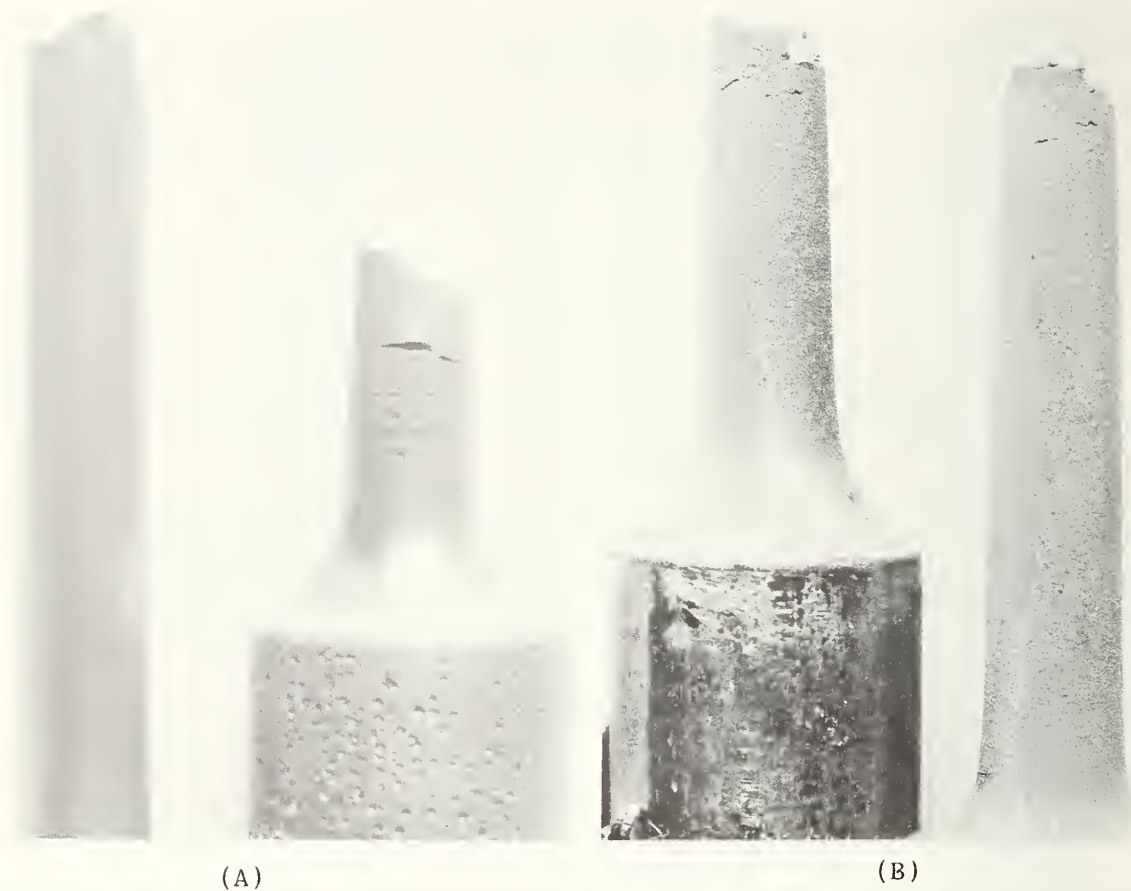


Fig. 1. Photographs of fractured 310 SS specimens tested in helium at 600°C at a strain rate of $10^{-6}/\text{s}$. (A) Nickel plated to a thickness of $62.5\mu\text{m}$. (B) Copper plated to a thickness of $100\mu\text{m}$. Magnification: 4X.

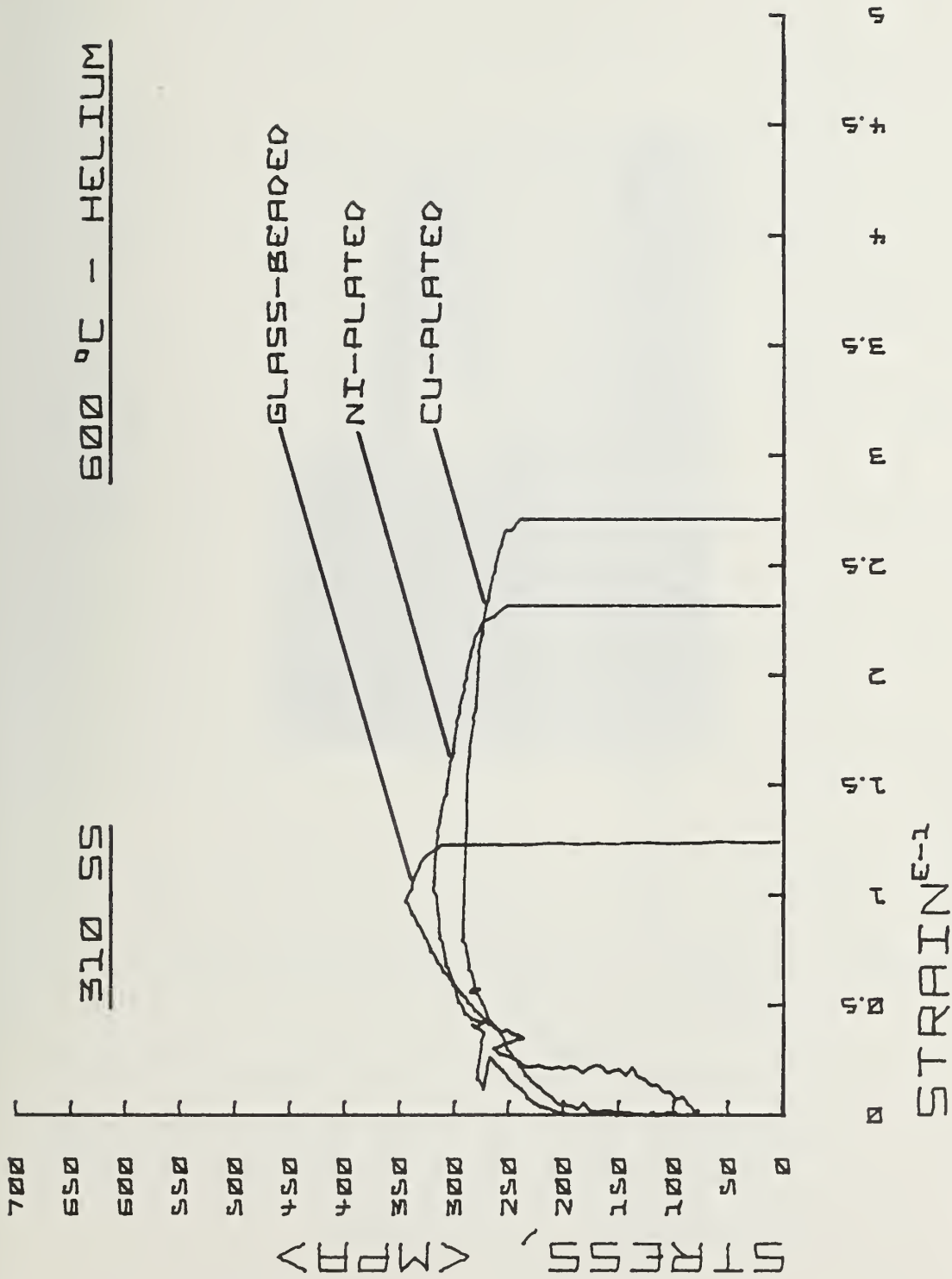


Fig. 2. Stress-strain curves of Type 310 SS specimens tested at a strain rate of 10^{-6} /s.



Fig. 3. Photograph of fractured 309 SS specimen tested in argon at 600°C at a strain rate of $10^{-6}/s$. Magnification: 5X.

600 °C - HELIUM

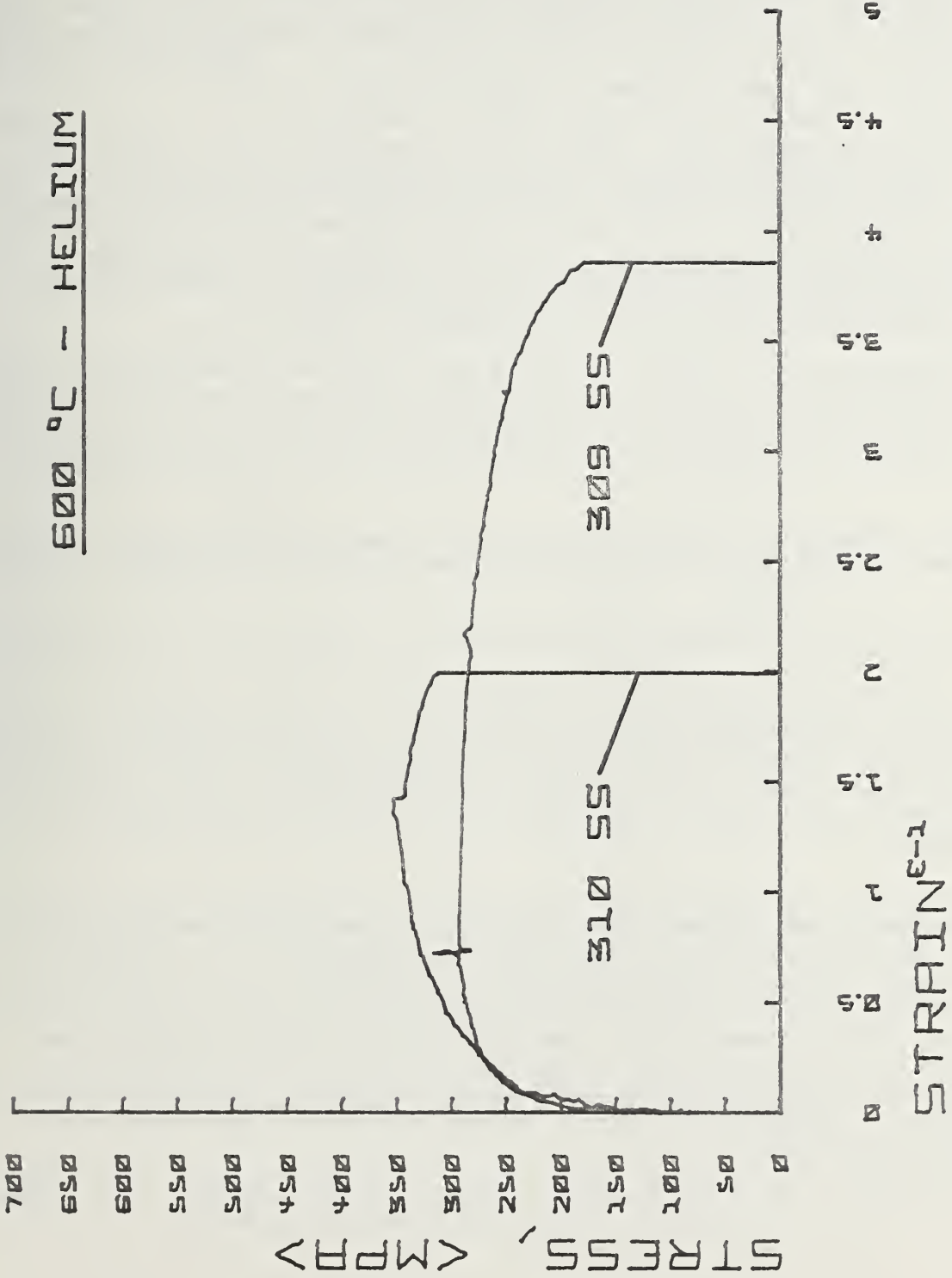


Fig. 4. Comparison stress-strain curves of Types 309 SS and 310 SS tested at a strain rate of 10^{-6} /s.

b. Pre-Cracked Fracture Test (J. H. Smith, 562)

Progress: Additional analysis of the tension loaded double cantilever-beam specimen was completed. Stress analysis programs were developed that are suitable for calculating the change in stress intensity with temperature, (K_T/K_O) , for a wide range of specimen materials, specimen configurations, specimen sizes, and initial stress intensity (K_O) . These stress analysis programs were used to extend the analysis shown in reference (1) to several candidate test materials which included 304, 310, 347 stainless steels, and Inconel 800. This analysis showed that the initial stress intensity level (K_O) can be varied over a sufficiently wide range, (up to 100 ksi $\sqrt{\text{in}}$) for typical specimen, and that the ratio (K_T/K_O) can be maintained equal to 1.0 up to approximately 600°C when the size and material in the specimen grips are properly chosen. In all cases, type 18-8 stainless steel is the optimum material for the loading fixture because it has a high coefficient of thermal expansion.

Optimization of the tension-loaded double cantilever beam specimen included a sensitivity analysis to determine what effect small changes in loading fixture length (L_F) , initial stress-intensity level (K_O) , and coefficients of expansion (α) has on the variation of the ratio $\frac{K_T}{K_O}$ with temperature.

These analyses show that when the initial loading fixture length (L_F) is chosen so that $\frac{K_T}{K_O}$ is independent of temperature, that changes of $\frac{K_T}{K_O}$ as much as 10% in L_F do not change $\frac{K_T}{K_O}$ more than 2%. Variations in the coefficients of expansion of the specimen, loading grips, or loading fixtures of less than 10% (the maximum expected variation for a given material) do not cause more than 2% variation in (K_T/K_O) . The ratio (K_T/K_O) is quite sensitive to the initial stress intensity value (K_O) and require that the length of the loading fixture (L_F) , be adjusted as the initial stress intensity (K_O) is varied.

Experimental tests to verify the analysis of the tension loaded double cantilever beam specimen were initiated. To verify the analysis of the specimen, the variation of the load-line displacement, V , and modulus of elasticity with temperature must be determined. This verification can be easily carried out with a metal having a low modulus of elasticity, a large change of modulus with temperature (dE/dT) , and a large initial load-line displacement (V_O) . Therefore, the initial verification tests can best be carried out using an aluminum specimen to verify the stress analysis. Subsequent tests will be carried out at higher temperatures with Ni-Cr alloys.

Initial tests were planned to use pre-cracked fracture mechanics specimens to conduct cracking tests in severe environments. These initial tests will include testing 304 and 347 type stainless steels in a chloride environment at temperatures to 600°C. Subsequent tests will include in addition type 310 stainless steel and will be conducted in a sulfidizing/oxidizing environment.

Plans:

1. Additional specimen development will complete the analysis of other test specimens and the sensitivity analysis. Elastic and creep strains will be included in the analysis.
2. The experimental verification of the stress analysis will be conducted.
3. Initial tests of a series of stainless steel alloys will be conducted.

Reference 1: Quarterly Report, Jan. 1 - March 31, 1978, p. 12 "Materials for Clean Utilization of Coal," EA 6010-15.

2. Ceramic Deformation, Fracture, and Erosion (E. R. Fuller, Jr., S. M. Wiederhorn, J. M. Bukowski, C. R. Robbins, and D. E. Roberts, 562.00)

Progress: Construction and assembly of the high-temperature, high-pressure mechanical loader was completed this quarter. This equipment is capable of mechanical property measurements at elevated temperatures and elevated pressures in the presence of simulated coal gasification environments. It remains, however, to establish and to optimize the operating characteristics of a pressure-balancing subsystem, and to determine the operational characteristics of the system as a whole.

The final phase of construction, completed this quarter, was the assembly and installation of the electronic pressure-balancing unit. This unit is required to minimize the pressure differential between the inner environmental chamber and the outer pressure vessel. The unit senses the pressure differential between the two chambers and, depending on the sign of pressure differential, controls two motor-driven metering valves. One of these valves admits a pressurizing gas into the outer pressure vessel to increase its pressure with respect to the inner chamber, whereas the other valve vents the containing gas from the outer pressure vessel to reduce its pressure.

Satisfactory operation of this pressure-balancing system has been established using two lengths of pressure tubing to simulate the two pressure chambers. (The tubing is actually the inlet plumbing to each of the two pressure chambers.) Although no attempt was made to optimize the controlling characteristics for this simplified test system, results were very encouraging. For an applied pressure of approximately 0.7 MPa (100 psi), the controllability was ± 0.007 MPa (± 1 psi). Upon increasing the operating pressure to approximately 4 MPa (600 psi), a 1% controllability was maintained, i.e., ± 0.04 MPa (± 6 psi). We expect that the increased volume of the actual vessels will somewhat dampen the response and minimize this pressure differential even further.

In addition to the above-mentioned equipment construction, a study was undertaken this quarter to examine the elevated temperature properties of two low-alumina refractory concretes after they had been exposed to a hydrothermal environment. The two laboratory refractory concrete compositions were composed of a calcined kaolin aggregate and either a high-purity or medium-purity calcium aluminate cement. The refractory concrete formulated with the high-purity and medium-purity cements are denoted A56 and A50, respectively, as they contain approximately 56 and 50 weight percent alumina. The cement to aggregate ratio (0.33) as well as the particle size distribution of the aggregate was the same for both refractories. The chemical composition of the two refractory concretes is given in Table 1.

Table 1 - Chemical Composition of Laboratory-Prepared Low-Alumina Refractory Concretes

	<u>A56</u>	<u>A50</u>
Alumina (Al ₂ O ₃)	55.6%	50.4%
Lime (CaO)	4.5%	8.4%
Silica (SiO ₂)	37.0%	38.4%
Iron Oxide (Fe ₂ O ₃)	0.8%	1.1%
Soda (Na ₂ O)	0.2%	0.1%
Others and Loss on Ignition	<u>1.9%</u>	<u>1.6%</u>
	100.0%	100.0%

Refractory concrete batches of 2000 grams were dry-mixed in a paddle mixer of 5 liter capacity until a homogeneous mixture was obtained. Water was added slowly to obtain the required workability for casting as determined by the "ball-in-hand" technique. The casting water used was 11.0 and 12.5 percent for the A56 and A50 compositions, respectively. Flexural strength bars (75 x 15 x 7.5 mm) were cast in gang molds coated with a silicone releasing agent. A combination of vibrating and tamping was used in placing the concrete in the molds. Immediately after casting, the molds were placed in a +95 percent relative humidity environment at a temperature of 22 to 25°C for 24 hours. The specimens were then removed from the molds, and dried for 48 hours at 110°C.

Samples treated hydrothermally were placed in a pressure vessel and heated to a temperature of 310°C in a saturated vapor environment of H₂O. After 65 hours, the temperature was increased to 610°C. Above the saturation temperature of 342°C during this heat-up, the steam was vented from the system to maintain the vapor pressure at 15.0 MPa (2180 psi). After exposure to temperature and pressure for 160 hours, the refractory concrete specimens were cooled to 500°C, where the hydrothermal environment was slowly vented to atmospheric pressure. During this venting the temperature decrease was typically 20 to 50°C. The specimens were then allowed to cool to room temperature.

The hot strength of the refractory concretes both before and after hydrothermal treatment was determined in four-point flexure on a universal testing machine. A constant crosshead displacement rate of 5×10^{-2} millimeters per minute was used throughout this study. All specimens were heated to the test temperature at approximately 5°C per minute. The specimens remained at the test temperature for 15 hours before measuring the high-temperature flexural strength.

The data for the hot strength, or hot modulus of rupture (MOR), are presented in Figures 1 and 2 for the A56 and the A50 refractory concretes, respectively. Similar to our studies at room temperature, these low-alumina refractory concretes exhibited a hot flexural strength after hydrothermal exposure that was 2 to 3 times greater than normally cured refractory specimens. The A56 refractory composition, which contains the high-purity calcium

aluminate cement, had the highest overall strength both before and after hydrothermal treatment. However, the largest relative increase in hot strength due to hydrothermal exposure was seen in the A50 refractory concrete at 1310°C.

The fractured surfaces of the refractory concretes before and after hydrothermal treatment are distinctly different. In the normally cured concretes, crack propagation and fracture occurred predominantly in the cement matrix, circumventing the aggregate grains. In the hydrothermally treated concretes, transgranular fracture of the aggregates was observed as the crack propagated through the refractory specimen. This indicates that the hydrothermal treatment has dramatically increased the strength of the cementing matrix as well as the cement-to-aggregate bond.

The erosion resistance of these refractory concretes was determined both at room temperature and at 1000°C. Particle speeds of 57 and 94 meters per second were used for these measurements. The abrading particles were 100 mesh silicon carbide particles and the impingement direction was normal to the surface being eroded. For each experiment, the erosion rate was determined from the total weight loss per unit weight of abrasive. A description of the erosion apparatus is given in Reference 1.

Initial results on the erosion resistance of the two low-alumina refractories are presented in Figure 3. Since each point represents only one specimen, the results indicate qualitative behavior requiring further quantitative confirmation. In all cases, the erosion rate of the normally cured low-alumina refractory (triangles) appears to be 2 to 3 times greater than similar specimens that were treated hydrothermally (squares). Filled and open symbols are used to denote the room temperature and 1000°C data, respectively.

Observation of the specimen surface after particle impingement provides a possible explanation for the differences in erosion rate. Erosion of the normally cured refractory occurs predominantly in the cementing matrix, as the cement is considerably weaker and more friable than the calcined kaolin aggregate. As the cement is removed, the aggregates are left standing in relief above the surface of the refractory, producing a channelling pattern of erosion. The protruding aggregate particles are bonded to the surface only by residual cement, and once this cement is removed, these particles also detach from the surface of the refractory. A slight rounding of the protruding calcined kaolin aggregate indicates that these particles are also being eroded by the silicon carbide, but at a much slower rate than the cement. The degree of channeling in the normally cured refractory concretes was greater in the A50 composition. In fact, the A56 composition exhibited hardly any channelling erosion in the 1000°C experiment.

The hydrothermally treated refractories did not exhibit this channeling phenomenon. Rather, the cementing matrix and the calcined kaolin aggregate appear to be eroded at approximately the same rate. This observation is in agreement with the strength data. Both indicate that the cementing matrix and the matrix-to-aggregate bond have become comparable in strength, and in erosion resistance, to that of the aggregate material.

Mineral phase changes were monitored by x-ray diffraction techniques at room temperature after the hot flexural strength determination. The results are tabulated in Tables 2 and 3. In general, hydrothermal exposure increases the reactivity of the free silica contained in the low-alumina refractory concretes. This free silica reacts with the calcium aluminate phases in the cement at approximately 300°C to form a hexagonal anorthite phase [CAS₂(H)]*. The hexagonal anorthite phase forms a strong, continuous structure of small crystallites that permeate the refractory matrix, and accounts for its high strength. At a temperature of approximately 1000°C in air, the hexagonal anorthite phase begins to transform to the more common triclinic form of anorthite [CAS₂(T)]. Room temperature x-ray analysis of hot MOR specimens shows that this transformation has gone to completion in 15 hours at 1210°C.

The mineral phases present at 1210°C, and above, in both the normally and hydrothermally cured refractories, are the same. This suggests that a controlling factor in the observed improvement in mechanical properties at elevated temperatures is not so much the phase assemblage, but rather, the path taken to produce the given phase assemblage.

Plans: In the next quarter, final evaluation of the apparatus for mechanical property testing at elevated temperatures and pressures will be undertaken. The controlling characteristics of the pressure-balancing unit will be established, and then optimized, as a function of operating pressure. Operation of the load application system will then be established in the presence of an applied pressure. To prevent condensation of steam in the lower region of the environmental chamber, a small heater will be installed around the lower loading bellows. The temperature profile will then be determined as a function of applied pressure to provide a temperature calibration for the system. Upon completion of these checkout procedures, the system will be operational and studies will begin on refractory concretes under hydrothermal conditions.

* Cement Chemistry Notation: C=CaO, A=Al₂O₃, S=SiO₂

Determination of the high-temperature mechanical properties of two low-alumina (+50%) refractory concretes after hydrothermal exposure will be completed. Exposure studies will begin for a high and low-alumina refractory concrete in a 60% H₂O - 40% H₂ environment. Room temperature mechanical properties subsequent to exposure will be determined for both refractories. X-ray diffraction analysis and scanning electron microscopy (S E M) will be used to monitor mineralogical and microstructural changes that have occurred from exposure.

Table 2 - Mineral Phases in the A50 low-alumina refractory as determined by Room-Temperature X-Ray Diffraction Analysis. The symbol X denotes the presence of the designated phase, whereas the symbol t denotes only a trace quantity.

	A ₃ S ₂	S(c) [*]	C ₂ AS	CAS ₂ (T) ⁺	CAS ₂ (H) ⁺	CA	CA ₂	CA ₆	C ₂ AH ₈	α-A
<u>A50 Normal</u>										
Room Temperature	X	X	X	t		X	X		X	
610°C	X	X	X	t		X	X			
1010°C	X	X	X	t		X	X			
1210°C	X	X	X	X			X	X		
1310°C	X	X	X	X				X		
<u>A50 Hydro</u>										
Room Temperature	X	X		X						X
610°C	X	X		X						X
1010°C	X	X		X						X
1210°C	X	X		X						X
1310°C	X	X		X						X

* S(c) = Cristobalite

+ CAS₂(T) = triclinic form and
CAS₂(H) = hexagonal form

Table 3 - Mineral Phases in the A56 low-alumina refractory as determined by Room Temperature X-Ray Diffraction Analysis. The symbol X denotes the presence of the designated phase, whereas the symbol t denotes only a trace quantity.

	A ₃ S ₂	S(c) [*]	C ₂ AS	CAS ₂ (T) ⁺	CAS ₂ (H) ⁺	CA	CA ₂	CA ₆	CAH ₈	α-A
<u>A56 Normal</u>										
Room Temperature	X	X		X		X			X	X
610°C	X	X		t			X			X
1010°C	X	X	t	X		X	t			X
1210°C	X	X	t	X			X			X
1310°C	X	X		X						X
<u>A56 Hydro</u>										
Room Temperature	X	X		t						X
610°C	X	X		t						X
1010°C	X	X		t						X
1210°C	X	X		X						X
1310°C	X	X		X						X

* S(c) = Cristobalite

+ CAS₂(T) = triclinic form and
CAS₂(H) = hexagonal form

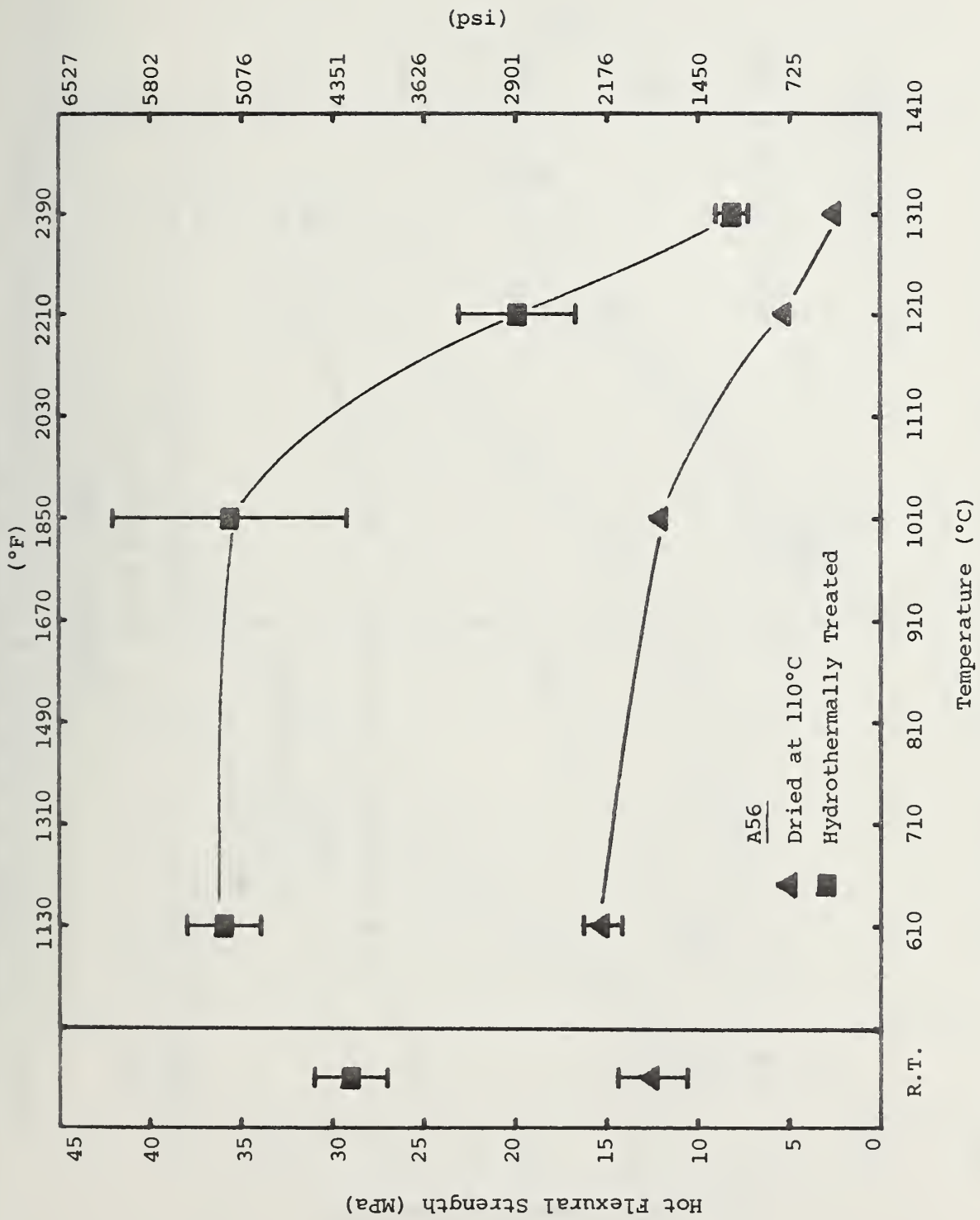


Figure 1. Hot flexural strength of a low-alumina (56%) refractory concrete both before and after hydrothermal exposure.

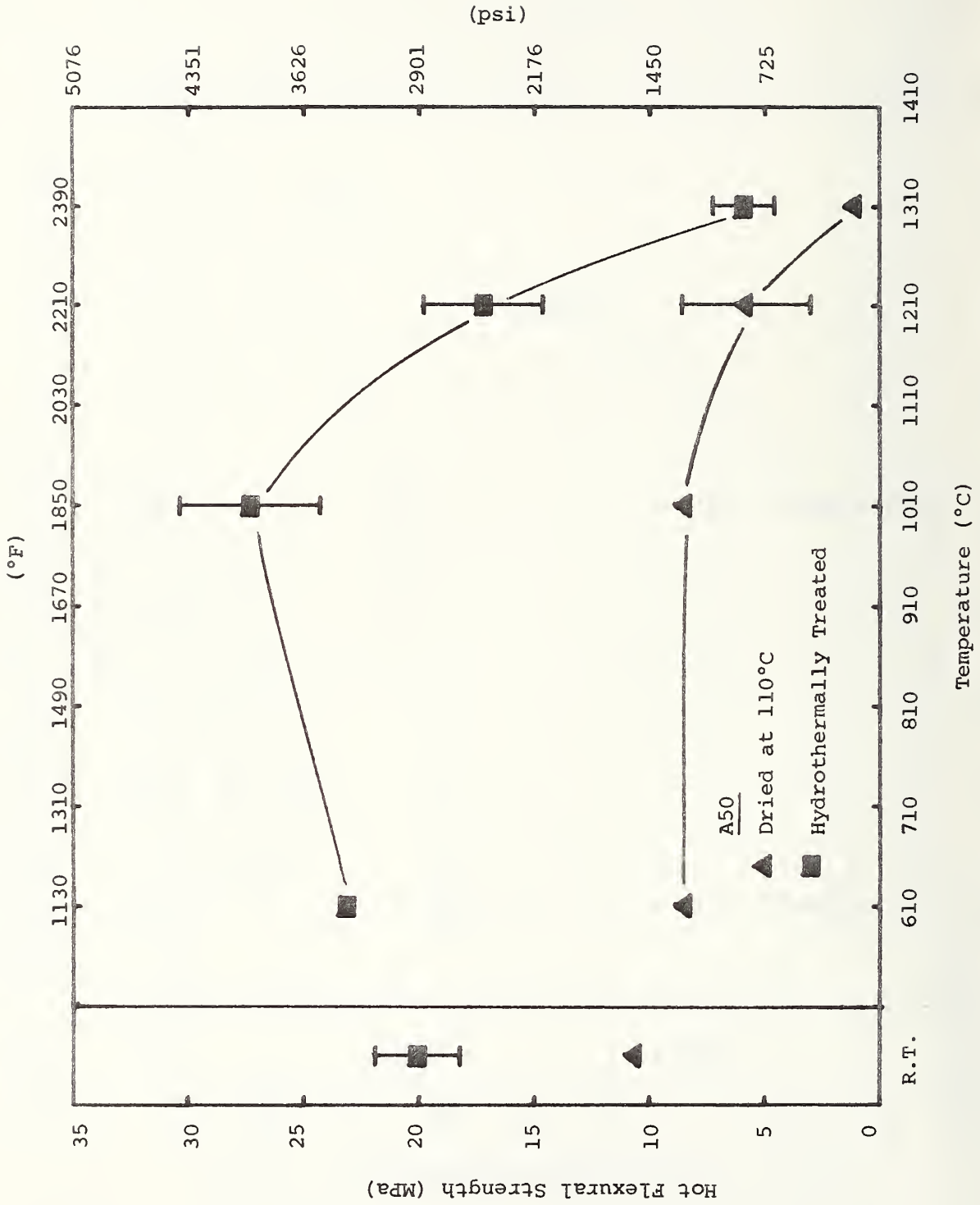


Figure 2. Hot flexural strength of a low-alumina (50%) refractory concrete both before and after hydrothermal exposure.

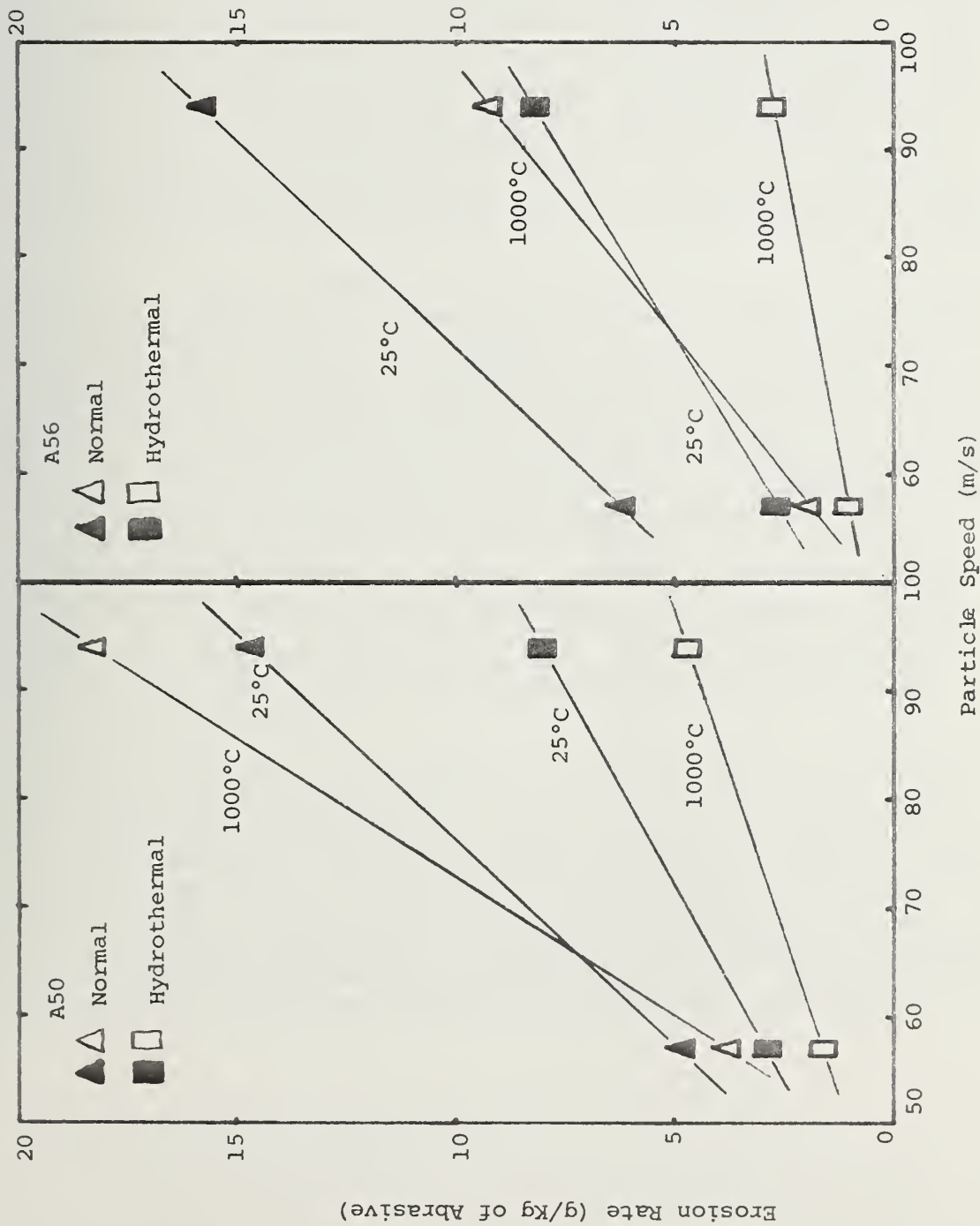


Figure 3. Erosion rate of low-alumina refractory concretes both before and after hydrothermal treatment.

Reference 1: Wiederhorn, S. M., and Roberts, D. E., "A Technique to Investigate High Temperature Erosion of Refractories," Bull. Am. Ceram. Soc., Vol. 55, 1976, pp 185-189.

3. Chemical Degradation of Ceramics

a. Reactions and Transformations (F. A. Mauer and C. R. Robbins, 565)

Progress: Three series of experiments were carried out using an unfired bar of high alumina neat cement (specimen #5) in a steam atmosphere. The specimen consisted initially of CA and α -A (major phases) with small amounts of CAH_{10} , C_2AH_8 , C_3AH_6 , and AH_3 . Study of this cement provides information on the chemical response of the bonding matrix of a high purity castable refractory to the steam in a gasification reactor environment. Phase assemblages were identified by visual inspection with the aid of standard reference patterns previously prepared, and by computer assisted analysis. A slight loss of pressure with time was detected early in the experimental sequence. Work was continued, however, because useful new information was being obtained even though the experimental conditions were somewhat different from those intended.

In the first series of experiments the sample was heated over a temperature range of 25-350 °C at pressures from ambient to 522 psig* for a total of 8 days. Results are summarized in Table 1. Hydration of CA was slight after 23 hrs. at 52 °C, but proceeded rapidly during the next 1.5 hours at 92 °C. After 2 additional hours at 93 °C, C_3AH_6 was readily identifiable and the amount of CA was greatly diminished. X-ray evidence indicates that CA hydrates much more readily than the aluminas present. After 3 hrs. at 150 °C, 60 psig all compounds in the assemblage C_3AH_6 , α -A, and AH were well crystallized. The amount of AH continued to increase through experiment 15 at 300 °C and 522 psig but, insufficient H_2O was present to hydrate all the α -A. At 241 °C and 308 psig, the C_3AH_6 phase was decreasing and a small amount of $C_4A_3H_3$ may have been present. At 300 °C and 480 psig, $C_4A_3H_3$, α -A and AH were the major phases. With an increase in temperature to 350 °C and a decrease in pressure to 350 psig, there was a marked decrease of bonding phase AH over a period of 5 hours.

A table of x-ray data is not given for the second group of experiments. The starting phase assemblage was $C_4A_3H_3$, α -A, and AH. The bonding phase $C_4A_3H_3$ was observed to be dissociating after 14 hours at 42 °C with the accompanying formation of bonding phase C_3AH_6 . After 3 hours at 93 °C, C_3AH_6 was the major phase and $C_4A_3H_3$ was present in only trace amounts. After 3 hours at 252 °C and 475 psig $C_4A_3H_3$ had reformed from dissociating C_3AH_6 , which is unstable in this temperature-pressure region. Further dissociation and reformation of these hydrated calcium aluminates was observed as temperature and pressure were varied.

* In SI units, 1 MPa \approx 145 psia.

Experimental results for the third series of experiments are summarized in Table 2. At the start of the experiment the bar was composed of $C_4A_3H_3$, α -A, and AH. At 103 °C after 20 hours of exposure the $C_4A_3H_3$ had completely dissociated to form C_3AH_6 . In experiment 40 the test bar was composed of C_3AH_6 , α -A, and AH, all well crystallized. Hydration of α -A was monitored by *in situ* x-ray diffraction as the temperature and pressure were gradually increased to 247 °C and 442 psig in experiment number 47. The amount of AH increased noticeably at 207 °C, 240 psig (experiment 45). At 235 °C and 410 psig (experiment 46) bonding phase C_3AH_6 was being replaced by bonding phase $C_4A_3H_3$, and bonding phase AH continued to form. At 247 °C and 442 psig (experiment 47) the specimen was essentially fully hydrated and the equilibrium phase assemblage was $C_4A_3H_3$, AH and a small amount of α -A. This assemblage was obtained to 354 °C, 715 psig (experiment 53), at which point AH was observed to have started to dissociate. Dissociation of AH continued as the temperature was slowly increased. At 448 °C, 520 psig (experiment 57) the rate of dissociation increased. Even at 550 °C, 542 psig (experiment 61) AH was present in the test bar as a minor phase. This temperature is roughly 200 °C above the "equilibrium" dissociation temperature commonly reported in the literature.

Hydration of the α -A of neat cement to form AH(boehmite), followed by dissociation of the latter as temperature is increased is illustrated by this series of experiments. Because of the dramatic loss of strength associated with the dissociation of the strong bonding phase, AH[†], the ability of the *in situ* x-ray method to observe the reaction in real time is of special interest. A series of four patterns showing the dissociation of AH are reproduced in Figure 1. The over-all change is shown in a difference plot (Figure 2) in which the negative peaks correspond to the AH phase consumed in the reaction, while the positive peaks show the increase in α -A, a reaction product.

Physical properties such as strength and erosion rate, which are affected by the presence of AH, can be expected to follow trends somewhat parallel to the formation or dissociation of this phase. For example, the flexural strength of the test bar used in this experiment (and, by analogy, a high purity refractory) might be expected to approach a maximum value at or near 354 °C and 715 psig under the conditions of this test. At higher temperatures, the strength should gradually decline as AH dissociates with slowly rising temperatures as shown in Figure 3. In this figure the intensity of an AH peak at channel 610 (solid line) and an α -A peak at channel 492 (dashed line) have been plotted for experiments 47 through 62 to show the trend in the relative amounts of these two phases.

[†] E. R. Fuller, Jr., C. R. Robbins, and A. Loeb, Quarterly Progress Report FE 1749-6, December 1975.

Rapid heating of a test bar (or refractory) would result in the superheating of AH followed by abrupt dissociation of the compound over a short temperature interval.

Plans: Twenty-five patterns obtained in a test of NBS refractory A-56 with mullite aggregate are now being analyzed. Test bars of a composition approximating that of the bonding matrix of A-56 have been prepared, and will be tested in steam. Work on both of these materials will be continued during the next quarter, along with additional work on specimens of neat cement.

TABLE 1 IN SITU X-RAY ANALYSIS OF UNFIRED HIGH ALUMINA NEAT CEMENT SPECIMEN #5 IN STEAM

EXPERIMENT NUMBER	TEMPERATURE (°C)	PRESSURE (psig)*	TIME (hr)	X-RAY ANALYSIS AND REMARKS
1	25			CA, α-A, major phases, traces of CAH ₁₀ , C ₂ AH ₈ , C ₃ AH ₆ , AH ₃
2	52		23	CA, α-A major phases, AH ₃ minor: CA slightly diminished
3	92		1.5	CA, α-A major phases: CA decreasing
4	93		2	CA, α-A major phases, AH ₃ minor: C ₃ AH ₆ forming, CA decreasing
5	94		13	C ₃ AH ₆ , α-A major phases, AH ₃ minor: AH forming
6	120		5	C ₃ AH ₆ , α-A major phases: AH forming †
7	150	60	3	C ₃ AH ₆ , α-A major phases: well crystallized †
8	150	60	2	ditto †
9	173	105	3	ditto †
10	168	105	14	ditto †
11	205	205	8	ditto †
12	205	182	20	ditto †
13	235	323	6	ditto †
14	241	308	23	C ₃ AH ₆ , α-A, AH: C ₃ AH ₆ decreasing †
15	300	522	4.5	C ₄ A ₃ H ₃ , α-A, AH, C ₃ AH ₆ †
16	300	480	10	C ₄ A ₃ H ₃ , α-A, AH, C ₃ AH ₆ trace †
17	350	350	5	C ₄ A ₃ H ₃ , α-A, AH
18	250			C ₄ A ₃ H ₃ , α-A, AH

* in SI units 1 MPa =145 psia

† Insufficient H₂O to Hydrate remaining α-A

TABLE 2 IN SITU X-RAY ANALYSIS OF UNFIRED HIGH ALUMINA NEAT CEMENT SPECIMEN # 5

EXPERIMENT NUMBER	TEMPERATURE (°C)	PRESSURE (psig) *	TIME (hr)	X-RAY ANALYSIS AND REMARKS
39	78		1	C ₄ A ₃ H ₃ , α-A, AH major phases
40	103		20	C ₃ AH ₆ , α-A, AH major phases
41	115		4	ditto
42	117		17	ditto
43	164	92	3	ditto
44	208	240	5	ditto
45	207	240	15	C ₃ AH ₆ , α-A, AH major phases: AH increasing
46	235	410	6	C ₄ A ₃ H ₃ , C ₃ AH ₆ , α-A, AH major phases: C ₃ AH ₆ decreasing, C ₄ A ₃ H ₃ , AH increasing
47	247	442	6	C ₄ A ₃ H ₃ , AH major phases, α-A minor phase
48	274	675	18	ditto
49	300	880	3.5	ditto
50	323	950	3	ditto
51	325	718	16	ditto
52	340	730	1	ditto
53	354	715	5	C ₄ A ₃ H ₃ , AH, major phases, α-A minor phases: α-A increasing, AH decreasing
54	375	540	21	C ₄ A ₃ H ₃ , α-A, AH major phases: α-A increasing, AH decreasing
55	400	520	4	ditto
56	428	522	0.5	ditto
57	448	520	1.3	ditto
59	525	535	1.3	ditto
61	550	532	1	C ₄ A ₃ H ₃ , α-A major phases, AH minor phase
62	650	570	1	C ₄ A ₃ H ₃ , α-A

* in SI units 1 MPa =145 psia

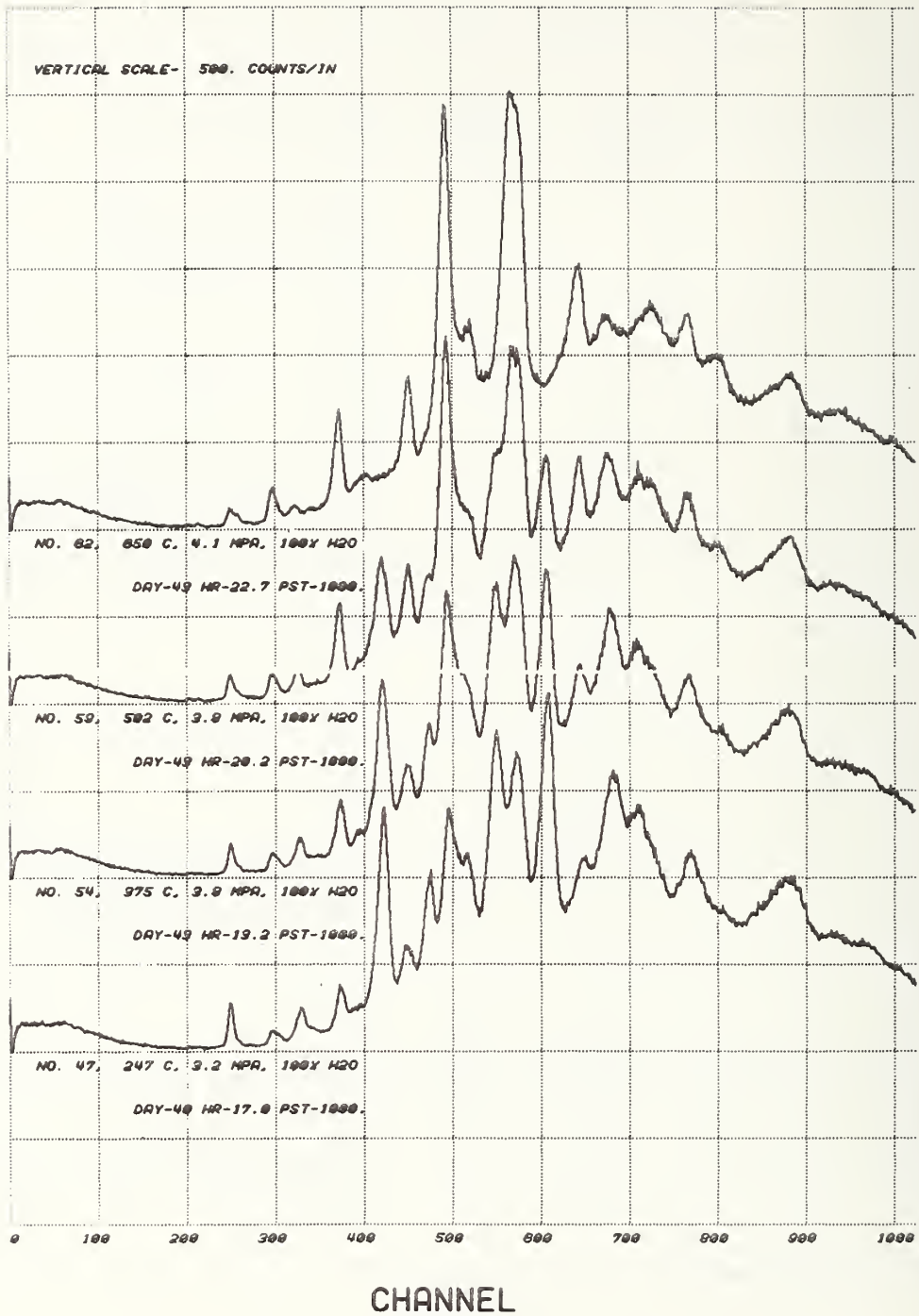


Figure 1. A series of four EDXD patterns showing the dissociation of AH (boehmite) and the formation of additional α -A in the temperature range 247° to 650°C.

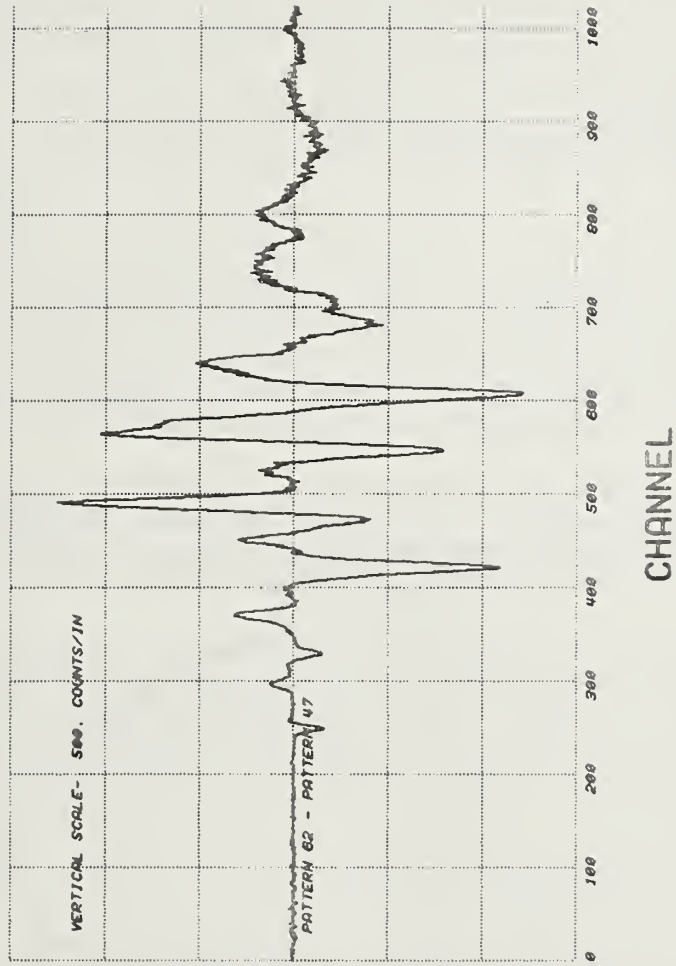


Figure 2. A difference plot (pattern 62 - pattern 47) showing the overall change in phase composition in the temperature range 247° to 650°C. The negative peaks correspond to the AH phase consumed in the reaction, while the positive peaks show the increase in the concentration of α -A, a reaction product.

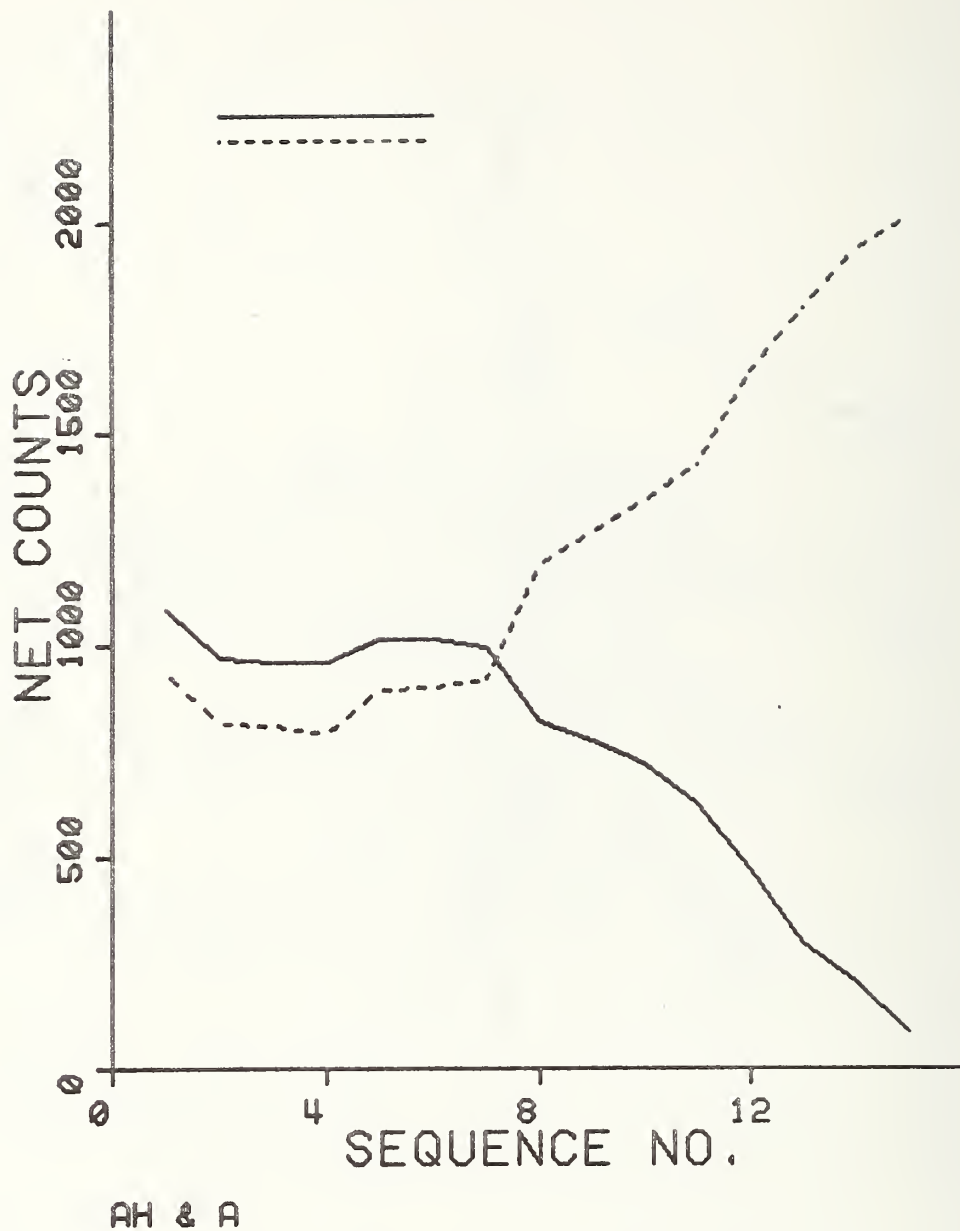


Figure 3. A plot of the intensities of an AH peak at channel 610 (solid line) and an α -A peak at channel 492 (dashed line) for experiments 47 through 62. The trends in the relative amounts of these two phases are shown.

b. Slag Characterization (W.S. Brower, J.L. Waring, C.A. Harding, and D.H. Blackburn, 565)

Progress: Previously it was reported that preliminary data appeared to indicate that the viscosity of a silicate melt increased with increasing steam pressure. Since no appreciable compositional deviations had apparently taken place in the slag, subsequent attempts were made to obtain more reliable data.

In the design used to gather the data which was reported previously, the temperature of the melt in the rotating crucible could not be measured directly and therefore was related to the temperature of the platinum heater.

An attempt was made to rectify this deficiency and thereby gain the precision of temperature measurement which is necessary to reproduce the data. A rotating thermocouple (Figure 1) was inserted through the rotating shaft and was allowed to touch the bottom of the melt crucible. This modification necessitated a complete redesign and change of the melt crucible and the entire driving mechanism.

To accurately measure viscosity, the vertical temperature gradients which exist in the melt must be established. This data is of particular importance in a pressure system where the ravages of steam cooling drastically effect the surface temperature of the melt.

In the first experiment, a vertical profile analysis, a thermocouple shielded with platinum was inserted into the melt at various depths. The temperatures at the different depths were recorded at a constant 55 psi and compared simultaneously with those of the platinum resistance heater and the bottom outside of the melt crucible. The results of this experiment are given in Figure 2. The data are plotted $T^{\circ}C$ vs Δ time in minutes - of the platinum heater (curve 1), of the vertical thermocouple probe (curve 2), of the bottom thermocouple (curve 3). In addition the depth of the vertical probe is shown as a superimposed upper ordinate. The values shown on curves 1 and 3 remain relatively constant. The values shown on curve 2 are at a maximum in temperature at about 1" depth (vertical midpoint of melt) with cooling at the top and bottom surfaces. From this profile it can be concluded that the bob must be placed at the approximate vertical center of the crucible and that a thermocouple placed at any other place in the melt will not reflect a representative melt temperature.

In the second experiment the vertical thermocouple probe was placed at 1" in the melt and the melt temperature was related to the platinum heater thermocouple and to the bottom thermocouple. The results are given in Table 1.

From Table 1 several things are immediately apparent. The difference between the temperature at the center of the melt and the bottom of the crucible (last column) is significantly large and relatively constant over the range of temperatures. Secondly, when the heater is operating at 1445°C and 60 psi, only 1201°C was achieved in the melt.

Using the information obtained in experiments one and two the viscosity (experiment 3) of the same slag as used previously was redetermined and the results are given in Table 2. The summation of these data (curve E) and how they are related to the previous data are shown in Figure 3. The new viscosity data, curve E, might have been expected to approximate closely curve B, but does not. When the temperature of the platinum heaters and of the bottom thermocouple in experiment 2 (Table 1) are compared with the values found in experiment 2 (Table 2) a great variation is found to exist between bottom thermocouple temperatures for the same platinum heater temperature. This apparent non-reproducibility of temperatures from experiment to experiment casts doubt on the validity of the viscosity measurement.

To reconcile this situation, an attempt was made to determine if something had changed radically in the experimental set up. Experiment 4, a duplication of experiment 2, was completed and the results are given in Table 3. The results of experiment 4 essentially duplicate those of experiment 2. The significant difference between experiments 3 and 2,4 is that in the calibration experiments (2,4) the thermocouple does not stir the melt with the vigor that the platinum bob does during viscosity measurements. The stirring action should cause a more uniform heat transfer to the bottom of the melt crucible and it follows that the temperatures observed while using the bob should more closely approximate the true temperature of the melt. However, these temperatures are not the true melt temperatures because of the steam cooling of the bottom surface.

Plans: Experiment 4 will be duplicated with a probe thermocouple with stirring fins to determine the effects of stirring on the heat transfer of the bottom thermocouple. A new suspension will be designed employing a thermocouple which is part of the bob for direct temperature measurement of the slag while measuring viscosity.

Table 1. Calibration of Melt at 61 psi Steam.

Δ Time	Platinum Heater Thermocouple	Thermocouple Immersed in Melt	Thermocouple Touching Bottom of Melt Crucible	Difference*
min	°C	°C	°C	°C
80	1302	1046	909	137
120	1377	1121	988	133
180	1434	1190	1068	122
240	1445	1201	1080	121

* Thermocouple temperature immersed in melt minus thermocouple touching bottom of melt crucible.

Table 2. Redetermination of Viscosity of Synthetic Slag* at 57 psi.

Platinum Heater Thermocouple	Thermocouple Touching Bottom of Melt	log η
°C	°C	
1305	1024	2.09
1377	1059	1.89
1434	1115	1.74

* Composition

	wt %
SiO ₂	42
Al ₂ O ₃	3
Fe ₂ O ₃	25
CaO	5
MgO	5
Na ₂ O	15
K ₂ O	5

Table 3. Recalibration of Melt at 63 psi Steam.

Δ Time	Platinum Heater Thermocouple	Thermocouple Immersed in Melt	Thermocouple Touching Bottom of Melt Crucible	Difference
min	°C	°C	°C	°C
80	1301	1042	921	121
120	1377	1113	990	123
180	1436	1167	1055	112

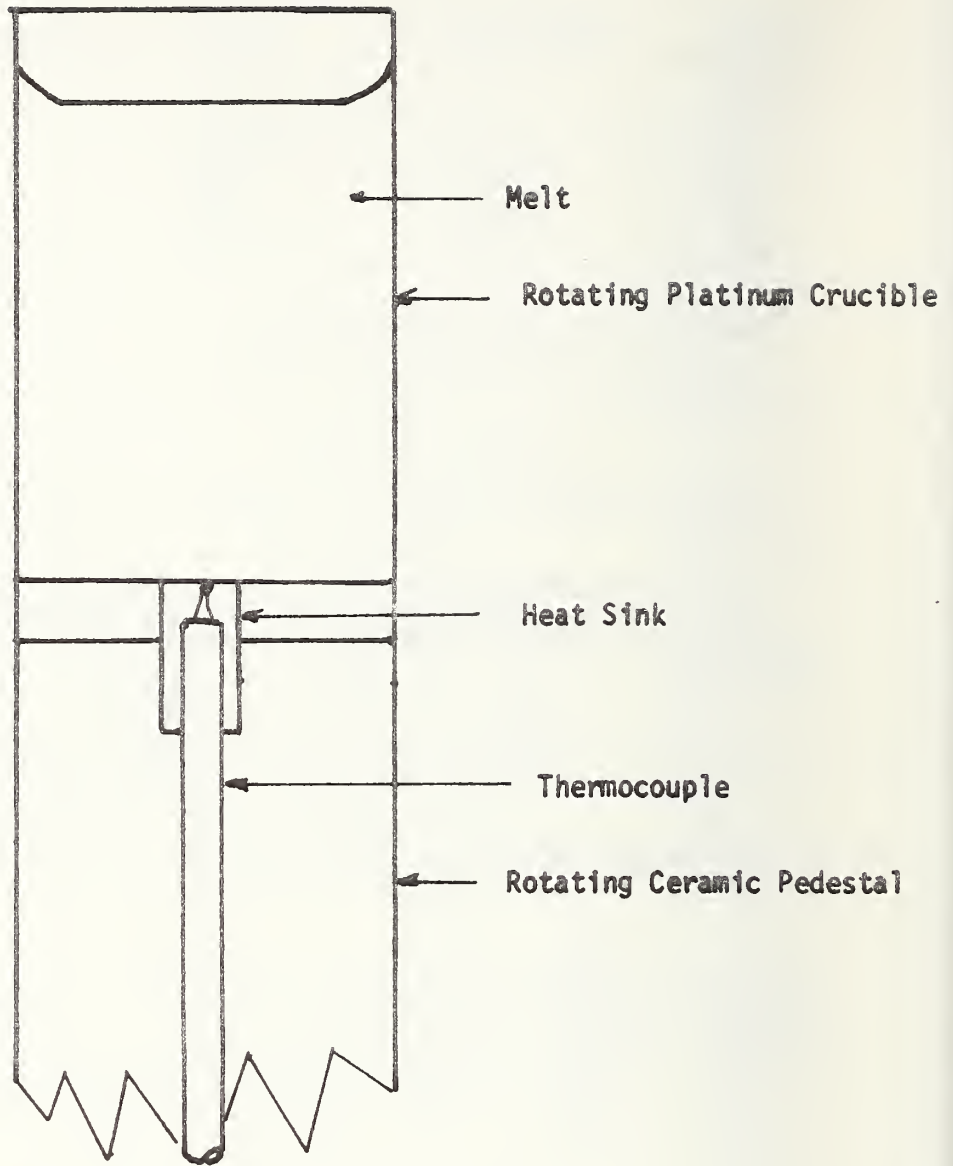


Figure 1. Rotating thermocouple assembly.

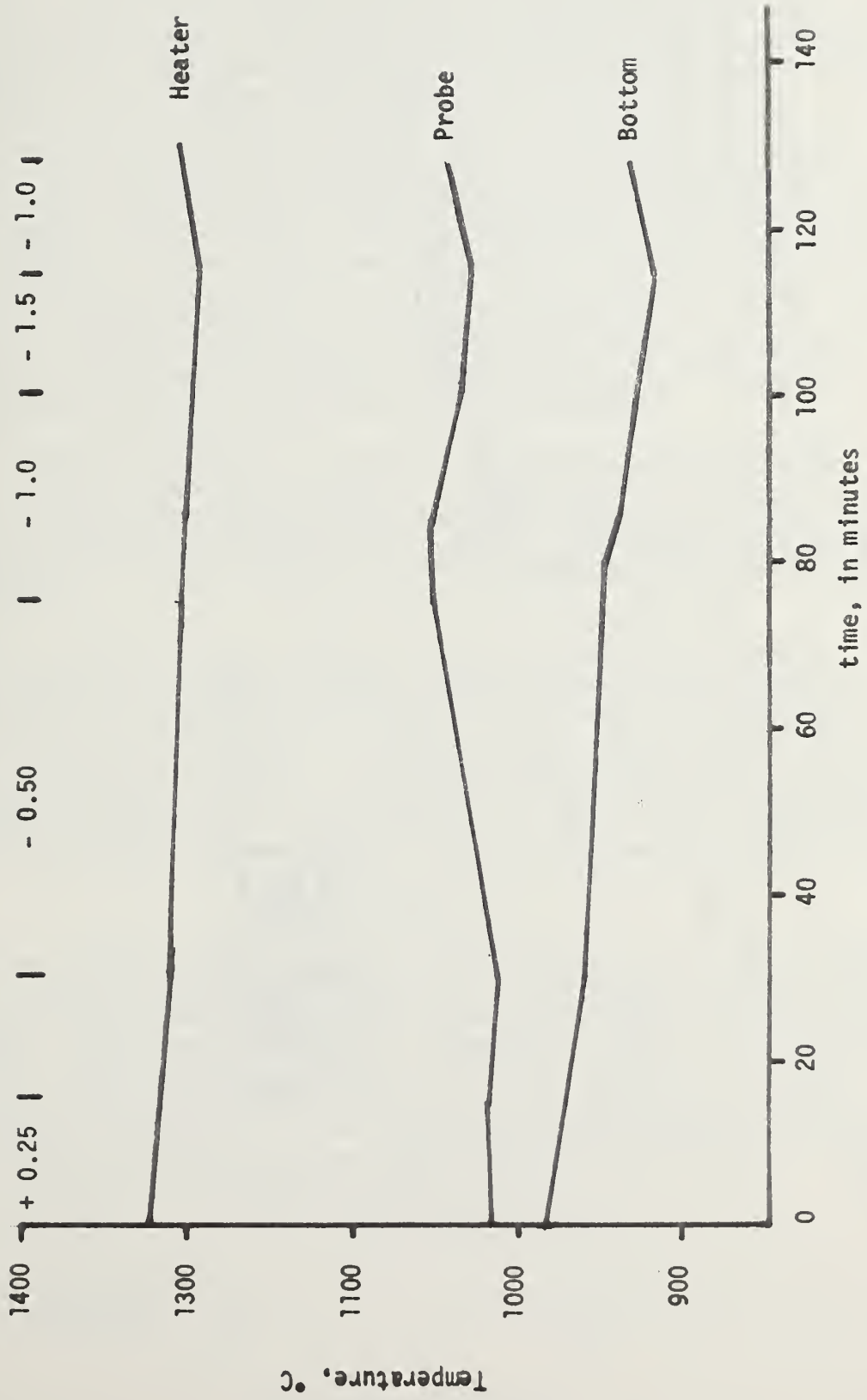


Figure 2. Vertical temperature profile of melt crucible.

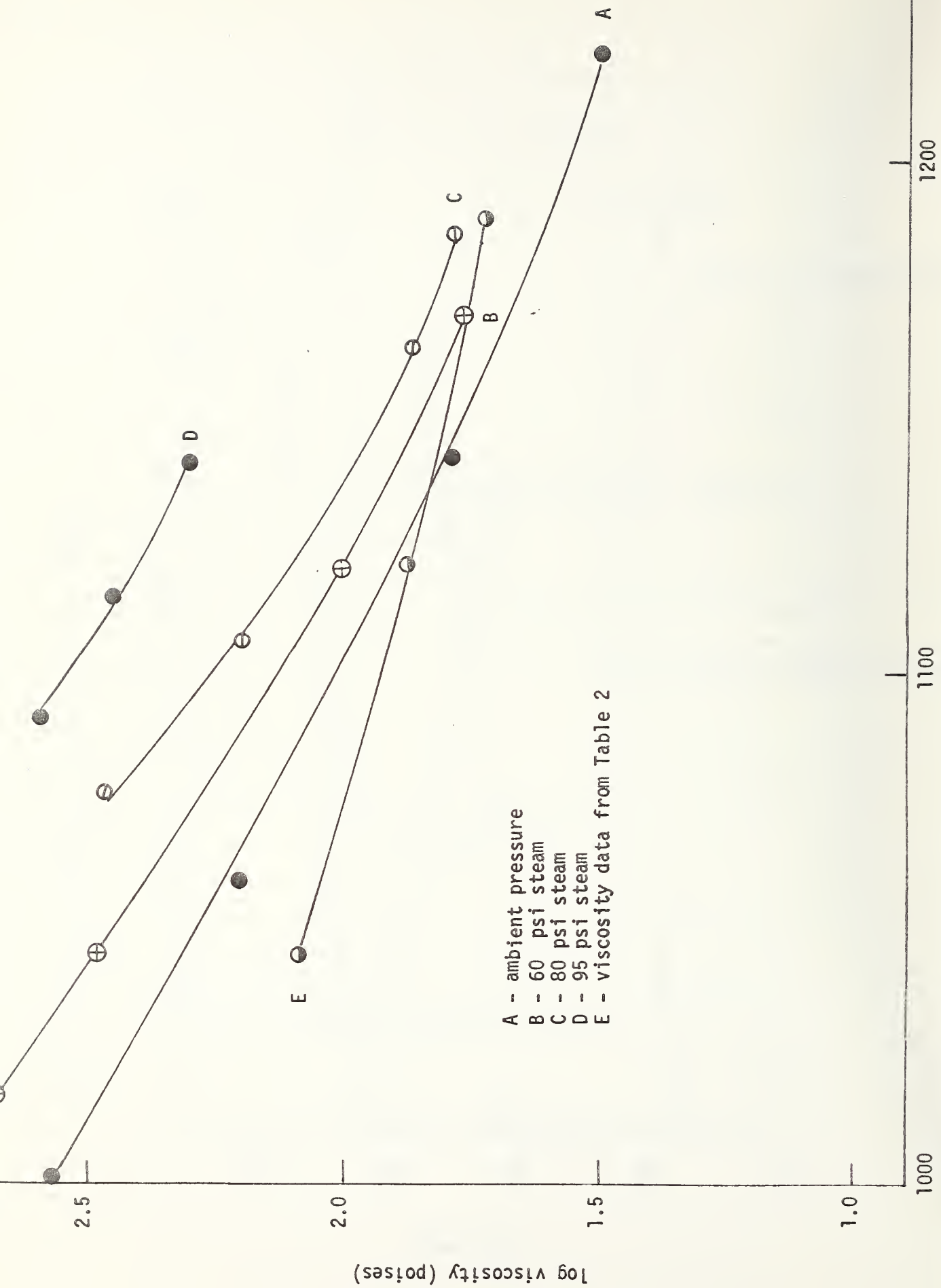
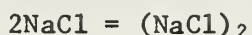


Figure 3. Log viscosity vs temperature for slag.

Progress: In the previous Quarterly report we presented experimental data, in the form of a mass spectrum, for an alkali silicate vaporization experiment. A thermodynamic calculation for the vaporization of this system has now been made using the JANAF (1971) Thermochemical Tables data base. The results indicated the presence of Na, NaOH and NaCl in the vapor phase. This contrasts with the experimental data where only Na was definitely identified. Similar thermodynamic calculations indicate that Na₂SO₄ should vaporize as NaOH in the presence of H₂O vapor. Using the capillary probe sampler we monitored this possible effect at temperatures of 1000-1200°C and an H₂O partial pressure of 28 torr in 1 atm* of N₂. No NaOH vapor was seen, with Na and SO₂ being the main vapor species. To test whether the absence of NaOH vapor species may be due to NaOH being dissolved at very low activity in the Na₂SO₄ melt, we carried out a separate series of vapor transport measurements over a NaSO₄ + 6wt% NaOH substrate. At 1000°C large amounts of NaOH and Na were found in the vapor, indicating a high activity for NaOH in this system. Hence the H₂O + Na₂SO₄ reaction seems to be kinetically hindered, and is not the result of a strong interaction between NaOH and Na₂SO₄ in the liquid. This result also probably explains the nonobservation of NaOH and NaCl vapor during the alkali silicate vaporization experiment.

A rather startling, but not yet repeated, effect was noted during the Na₂SO₄ + NaOH vaporization experiment. The presence of NaOH seemed to markedly increase the loss of Na₂SO₄ but not as SO₂, Na or Na₂SO₄. Perhaps a new as yet unidentified molecule is formed in the presence of NaOH. Also during this study the capillary probe plugged as the result of apparent Pt transport.

In order to verify that the observed lack of activity of H₂O with Na bearing liquids is a chemical kinetic phenomenon and not a sampling probe perturbation of the data the following test was made. We should recall from our earlier studies that the conical type of sampling probe did not perturb equilibrium processes. However the capillary probe used for the most recent experiments had not been tested for its ability to sample equilibrium systems without perturbation. A critical test of sampling fidelity is provided by measurements of the vapor phase dimerization process:



as was done earlier for the original conical probes. Using the capillary probe we obtained vapor pressure data for the species NaCl and (NaCl)₂ from which the apparent equilibrium constant for the above reaction was determined. Data were obtained over a temperature interval of 1100-1500K and an NaCl partial pressure range of 10⁻³ - 10⁻¹ atm in 0.5 atm N₂ carrier gas. The results shown in Fig. 1 are in good agreement with the JANAF Thermochemical Tables data for an equilibrium process. Hence the sampling probe does not perturb the system and the observed non-equilibrium effects for H₂O reactions are inherently chemical kinetic.

*1 atm = 101,325 Pa

1 Torr = $\left(\frac{101,325}{760}\right)$ Pa

Plans: In the following Quarter we plan to present a paper on the new transpiration mass spectrometric technique, and its application to high temperature - high pressure vapor transport measurement, at the 10th Materials Research Symposium on Characterization of High Temperature Vapors (NBS Sept 18-22, 1978). As this will be the first formal presentation and publication of the technique, our efforts during the next Quarter will emphasize demonstration of the method using the well defined calibration systems of Na_2SO_4 and NaCl . The merits of various types of sampling nozzles and the applicable range of temperature and pressure will be investigated during the period.

Following completion of this evaluation and publication activity work will resume on the slag-type mixtures using the capillary sampling probe system. The new vacuum system designed for vertical sampling of greater than atmospheric pressure systems should also be ready for laboratory installation during this period.

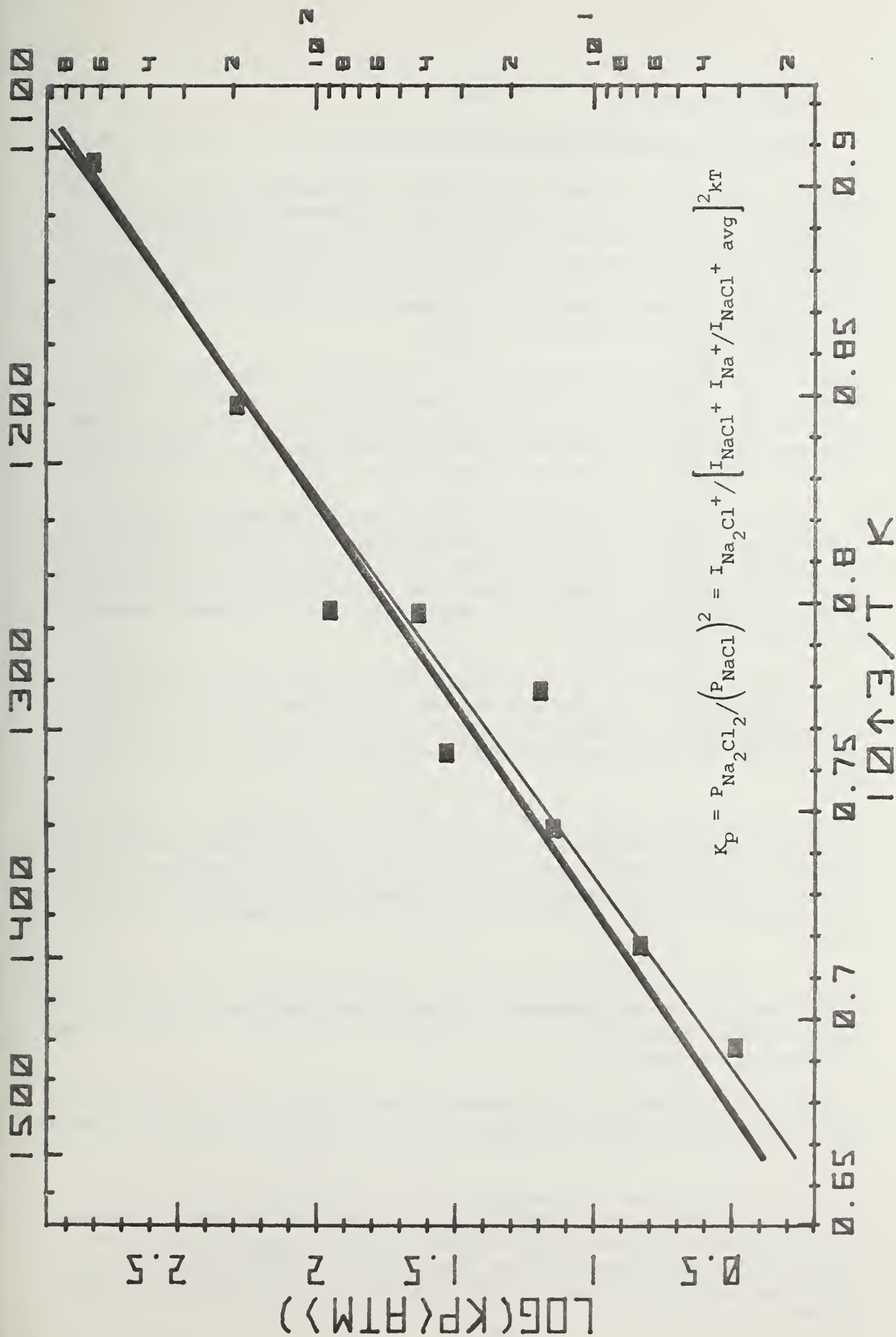


Figure 1: Plot of equilibrium constant for the vapor phase process: $2\text{NaCl} - (\text{NaCl})_2$ as a function of temperature using a capillary probe; heavy line — JANAF Thermochemical Tables data; thin line — least squares fit of data points.

4. Failure Prevention

a. Failure Information Center (R. C. Dobbyn and W. A. Willard, 562)

Progress: During the quarter the Failure Information Center received 32 reports of operational experiences and components and materials failures in coal conversion pilot plants and process development units. This number includes several diagnostic failure analyses from Argonne National Laboratories and Oak Ridge National Laboratories. To date, the percent contribution of information items received from different coal conversion processes is shown in Table 1.

These reports have been classified and evaluated for technical completeness and accuracy and discrepancies have been resolved. Detailed abstracts of this information have been entered into the Center's computerized data bank. A recent update of the frequency of failure modes, which analyzes all information in the system, is shown in Table 2.

The Information Center continued to aid Battelle-Columbus in their preparation of the DOE Materials and Components Newsletter feature on failure experiences. Weekly updates of all abstracts are furnished to Battelle together with complete hard copy of certain reports when requested. During the quarter, the Center furnished 20 updated summaries and 42 complete reports.

The Information Center also handled 19 other requests for information during the quarter. In response to these inquiries, copies of 203 abstracts, hard copy and draft reports were transmitted. In addition, 8 visitors to the Center were briefed on its scope, operation and future plans.

During this quarter major emphasis continued to be placed on completing the final report covering the performance of materials and components at the Conoco lignite gasification pilot plant - the CO₂ Acceptor Process. The draft report is now approximately seventy percent complete; delivery of the report to DOE and Conoco for review is now scheduled for mid - August.

Plans: Plans for the next quarter include completion of the final report covering the CO₂ Acceptor Process pilot plant and a similar, but less detailed, report covering the operating experiences to date at the IGT Hygas pilot plant.

In addition, liaison with the remaining gasification and liquefaction pilot plants and process development units - those not yet visited--will continue.

The format of failure data entries is being revised to facilitate information exchange and further, in-depth analysis of common problems. These analyses will become the subject of future reports issued periodically and supplied to DOE for distribution. Submittal of candidate topics and report outlines for DOE concurrence is also planned during the next quarter.

TABLE 1

COAL CONVERSION PROCESSES

NO OF ITEMS	PERCENT	PROCESS
17	3.86	BIGAS
1	0.22	BIOMASS
37	8.40	BMI
7	1.59	CARBONATE
17	3.86	CLEAN COKE
1	0.22	COED
54	12.27	CO2
2	0.45	CPC
12	2.72	CRESAP
2	0.45	EXXON
3	0.68	GFERC
57	12.95	HYGAS
1	0.22	LERC
11	2.50	LIGNITE
19	4.31	MERC
24	5.45	MISC.
2	0.45	PERC
22	5.00	SRC
6	1.36	SRC-W
111	25.22	SYNTHANE
4	0.90	SYNTHOIL
30	6.81	WESTINGHOUSE

440 = TOTAL NUMBER OF ITEMS IN FILE

TABLE 2

NUMBER OF REPORTED INCIDENTS OF FAILURES
IN COAL CONVERSION PLANTS

FAILURE MODE	FAILURE MODE ANALYSIS											TOTAL
	COAL CONVERSION PROCESS											
	BIGAS	BATTELLE	CO ₂	CRESAP	HYGAS	SRC	SYNTHANE	WESTING- HOUSE	OTHER			
CORROSION	0	2	37	4	30	8	22	6	42		151	
AQUEOUS	0	0	0	0	1	0	0	0	3		4	
CARBURIZATION	0	0	8	0	1	0	0	1	2		12	
METAL DUSTING	0	0	4	0	0	0	0	0	3		7	
OXIDATION	0	0	2	0	4	0	0	1	4		11	
FITTING	0	0	3	1	4	3	6	0	8		25	
SULFIDATION	0	0	13	0	12	0	6	1	4		36	
GENERAL	0	2	7	3	8	5	10	3	18		56	
EROSION	2	4	7	9	12	6	26	6	20		92	
EQUIPMENT MALFUNCTION*	5	4	6	3	9	2	9	2	6		46	
MANUFACTURING DEFECT	8	10	11	9	7	8	28	5	19		105	
DESIGN	5	6	5	8	4	8	17	5	14		72	
FABRICATION	0	1	3	0	2	0	4	0	2		12	
QUALITY CONTROL	3	3	3	1	1	0	7	0	3		21	
STRESS CORROSION	2	0	5	1	6	5	6	8	15		48	
CHLORIDE	0	0	4	0	6	2	4	0	9		25	
OTHER	2	0	1	1	0	3	2	8	6		23	
STRESS/TEMP. FAILURE	0	2	1	0	6	0	6	6	8		29	
CREEP	0	0	0	0	1	0	0	0	3		4	
FATIGUE	0	2	0	0	2	0	3	4	4		15	
THERMAL STRESS/SHOCK	0	0	1	0	3	0	3	2	1		10	

* FAILURES FROM TEMPERATURE/PRESSURE EXCURSIONS.

b. Materials Properties Data Center (H. M. Ondik and T. A. Hahn, 565, and I. J. Feinberg, 562)

Progress: The two computer terminals and the two acoustic couplers described in previous reports, have been delivered, but the telephone lines necessary for communication with a central computer have not yet been installed. Even though the terminals are not connected to a large computer, there are useful operations which may be performed, providing experience with the equipment and aiding in the data design. The "intelligent" terminal with cathode-ray tube display is particularly useful. Because this terminal has a small core storage memory it is possible to use it as a very small computer. As a result, the staff of the center has had opportunity to gain some familiarity with the detailed capability of the terminal with respect to its graphics handling capacity.

More equipment for the computer-terminal facility is now on order. A hard-copy unit, compatible with the "intelligent" terminal, will enable the operator to obtain a high-quality copy of material from the cathode-ray tube. Copies of graphs produced by the terminal and displayed on the tube will be available very simply with this copier.

A decision has been made as to the computer Data Base Management System (DBMS) to be used. The system of choice has the necessary system flexibility, an appropriate data storage structure including an inverted file system, an ad hoc query language necessary for ready searching, and suitably large storage capacity for the projected contents of the data bank. The DBMS is available from several GSA-approved commercial vendors.

Investigation and comparison of the services provided by these vendors is in progress. Arrangements have been made for short-term (the remainder of the fiscal year) use of the chosen DBMS through the services of two different vendors. Benchmark testing will be performed by building a small portion of the Data Base, storing the data on the computer, manipulating it, and searching it. These operations will test the system controls provided by the two vendors, and also compare the costs incurred during use of the two vendors' systems. The appropriate documents are being prepared for the justifications to obtain the various approvals required for contracting with a vendor.

Members of the staff have taken a one week course on the chosen DBMS, learning how data should be structured to make the best use of the capabilities of the system. Since each DBMS has its own special features, and complicated restrictions, it is necessary to have detailed instruction in its use. The chosen system, because of its large capability and flexibility, especially requires this special study and instruction so that it may be used efficiently. Inefficient use can drastically affect the computer expenditures.

The design features of the data bank are being planned. The arrangement of the data must take into account the varied types of information to be stored and the estimated order and frequency of requests for information. The optimum structure of the file for ready search capability must provide for the use of the fastest, therefore least expensive, search patterns compatible with flexibility, having as many items being searchable as possible for reasonable use. Major search elements will, of course, include the material names or designations and the properties. Searches must be possible on various combinations of these elements. The conditions under which the properties were studied must be retrievable along with the property data and should probably also be a searchable item as well. Many other items which must be appropriately entered for retrieval with the property data such as brief summaries of the test procedures, references, etc., must be considered carefully as possible candidates for keying as search categories. Since search items are carried in storage as inverted files and therefore, add to computer storage costs, the question of optimum use of the DBMS and its storage and query capabilities is an important one to answer carefully.

The first reports summarizing DOE contractors' reports have been submitted to DOE for approval of style, format, and content. These reports have gone through several revisions and are now considered to be in a form which can form the nucleus of the input to the data bank. The summaries condense the results of many reports into a concise form. Further reports now in progress will be completed when DOE approval of the first two is given.

Plans: The regular operations of the Center will continue with the handling and summarizing of the contractors' reports, the design of the structure of the data base, further study of the DBMS with respect to making optimum use of it, and also further study of the use of the computer terminal equipment as it arrives. The investigation of suitable vendors of the DBMS will continue so as to choose one as soon as possible.